Journal of Information Display, vol. 4, no. 1, 2003

A Defect Free Bistable C1 SSFLC Devices

Chenhui Wang and Philip J. Bos

Abstract

Recent progress in both low pretilt and high pretilt defect free C1 surface stabilized ferroelectric liquid crystal (SSFLC) devices is reviewed. First, by numerical calculation to investigate the balance between surface azimuthal anchoring energy and bulk elastic energy within the confined chevron layer geometry of C1 and C2, it is possible to achieve a zigzag free C1 state by low azimuthal anchoring alignment with a low pretilt angle. The critical azimuthal anchoring coefficient for defect free C1 state is calculated. Its relationship with elastic constant, chevron angle as well as surface topography effect are also discussed. Second, using 5 ° oblique SiO deposition alignment method a defect free, large memory angle, high contrast ratio and bistable C1 SSFLC display, which has potential for electronic paper applications has also been developed. The electro-optical properties and bistability of this device have been investigated. Various aspects of defect control are also discussed.

Keywords : liquid crystal display, surface stabilized ferroelectric liquid crystal (SSFLC), zigzags, electronic paper.

1. Introduction

Recently, the hand-held electronic products using novel displays with low power consumption and high contrast ratio have drawn more and more attention. Some liquid crystal based bistable displays, including cholesteric liquid crystal [1], bistable twist nematic (BTN) [2] and ferroelectric liquid crystalline polymers (FLCPs) [3] have been demonstrated. Ever since surface stabilized ferroelectric liquid crystal (SSFLC) was first introduced by Clark and Lagerwall [4] in 1980, bistable ferroelectric liquid crystal displays are potential candidates for E-paper application due to its fast response time, wide viewing angle, high contrast ratio and zero power consumption. Considerable work has been done on eliminating zig-zag defects for display applications. A large amount of this research has concentrated on determining which alignment materials and surface treatments tend to produce defect free texture. More recent papers by Kobayashi [5] et al., Koden [6] et al., Kanbe [7] et al., and Watson [8] et al. clearly explained the formation of zigzag defects in terms of pretilt angle α, cone angle θ_c, chevron angle δ and the surface topography effect. Zigzag formation occurs when domains with chevrons pointing in opposite directions are interspersed. Geometrically necessary conditions for formation of these configurations are: when $\alpha<\theta_c+\delta$, C1 is allowed; when $\alpha<\theta_c-\delta$, C2 is allowed. Normally, zigzag can be eliminated by a high pretilt. [4,9] Clearly, when the C2 condition is met, the C1 condition will also hold. That is the reason why it is hard to get zigzag free texture at low pretilt angle. Recently, Kurihara[10] *et al.* reported that they obtained zigzag free C1 SSFLC using photo alignment technique where obtained values of both the pretilt angle and the azimuthal anchoring energy are low. In this paper, our numerical calculation shows that it is possible to get zigzag free C1 state with low azimuthal anchoring at low pretilt angle. The critical azimuthal anchoring coefficient for defect free C1 state is calculated. Its relationship with elastic constant, chevron angle as well as surface topography effect are also discussed.

On the other hand, with an intermediate pretilt angle, a zigzag free C1 structure can be achieved [11]. However, this device still generally shows some defects. In this

Manuscript received February 19, 2003; accepted for publication March 20, 2003.
We would like to acknowledge Displaytech Inc. and NSF ALCOM grant, DMR 89-20147 for the equipment and financial support.
Corresponding Author : Philip J. Bos
Liquid Crystal Institute, Kent State University, Kent, Ohio 44242, USA.
E-mail : pbos@lci.kent.edu **Tel** : +1 330-672-2511 **Fax** : +1 330-672-2796

paper we show a defect free C1 SSFLC device with excellent bistability, high brightness, wide viewing angle and high contrast ratio, which has potential for E-paper applications. The methods to control and minimize the defects are also discussed.

2. Defect Free Bistable C1 SSFLC

The basic symmetric chevron layer structures of C1 and C2 states are shown in Fig. 1. The two boundary plates are equally treated and the rubbing directions of two plates are parallel. C1 is the structure where the chevron apex is pointing opposite to the rubbing direction; C2 is the structure where the chevron apex is pointing towards the rubbing direction. Zigzag formation occurs when domains with chevrons pointing in opposite directions are interspersed. Zigzag defects seriously degrade the quality of the electrooptical properties of the display. Geometrically necessary conditions for formation of these configurations are shown in Fig. 2: when $\alpha<\theta_c+\delta$, C1 is allowed; when $\alpha<\theta_c-\delta$, C2 is allowed. As described previously, when the C2 condition is met, the C1 condition will also hold. That is the reason why it is hard to get zigzag free texture at low pretilt angle. Apparently, zigzags can be eliminated by a high pretilt. 5° SiO deposition method normally generates uniform high pretilt alignment with the director lying parallel to the evaporation direction. Using obliquely evaporated SiO as alignment layer for nematic liquid crystal was first reported by Janning [12]. Bos [9] reported that they used high pretilt SiO alignment to achieve zigzag free C1 SSFLC. However, this device still generally shows some defects.

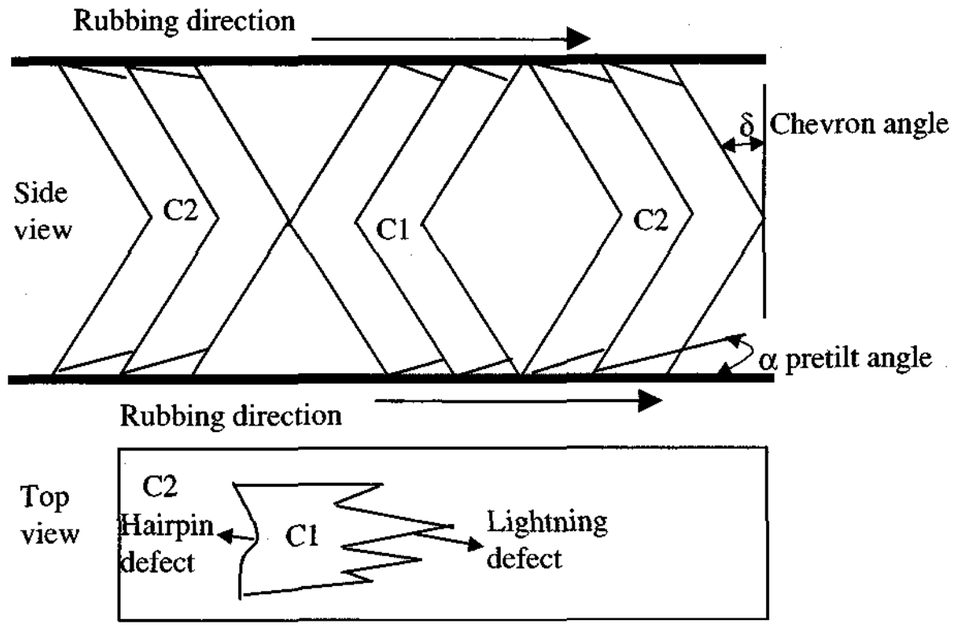

Fig. 1. Chevron structure of C1 and C2 states. The upper figure shows the chevron structure of uniform C1 and C2 states with pretilt angle α. And the lower figure shows the shape of a zigzag defect appearing on the top of the cell.

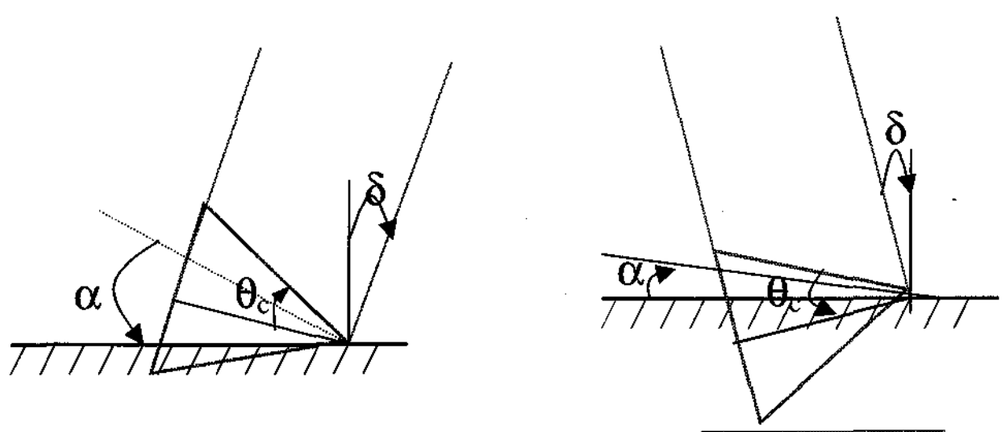

Fig. 2. Geometrical Conditions for C1 and C2 States.

3. Zigzag Free C1 with a Low Pretilt

3.1 Free energy of SSFLC

The total free energy per unit area **F** of SSFLC is given by [5,12]:

$$F = \int_0^d f_b dZ + f_s \qquad (1)$$

Where d is cell gap, $\mathbf{f_b}$ is the bulk free energy density and $\mathbf{f_s}$ is related to the surface anchoring energies including the chevron interface. We only consider the system without an electric field and at the chevron interface the director is horizontal. The expressions of $\mathbf{f_b}$ and $\mathbf{f_s}$ are given by equation 2 and 3 at this condition [5], where B_i (i=1, 2, 3, 13), ω, δ, W_a and φ are: elastic constants, angle between **Y**-axis and the projection of the director on the bounding plate, chevron angle (or layer tilt angle), azimuthal anchoring coefficient and azimuthal angle, respectively. The D1 term can be transformed into the surface energy term, which plays the same role as polar surface anchoring. The D term can also be transformed into surface energy term [5].

$$f_b = f_{elas} = \frac{1}{2}\left\{\left(B_1 \sin^2\varphi + B_2 \cos^2\varphi\right)\cos^2\delta + B_3 \sin^2\delta - 2B_{13} \sin\delta\cos\delta\sin\varphi\right\}\left(\frac{d\varphi}{dZ}\right)^2 + D_1 \cos\delta \sin\varphi \frac{d\varphi}{dZ} - D \sin\delta \sin\varphi \frac{d\varphi}{dZ} \qquad (2)$$

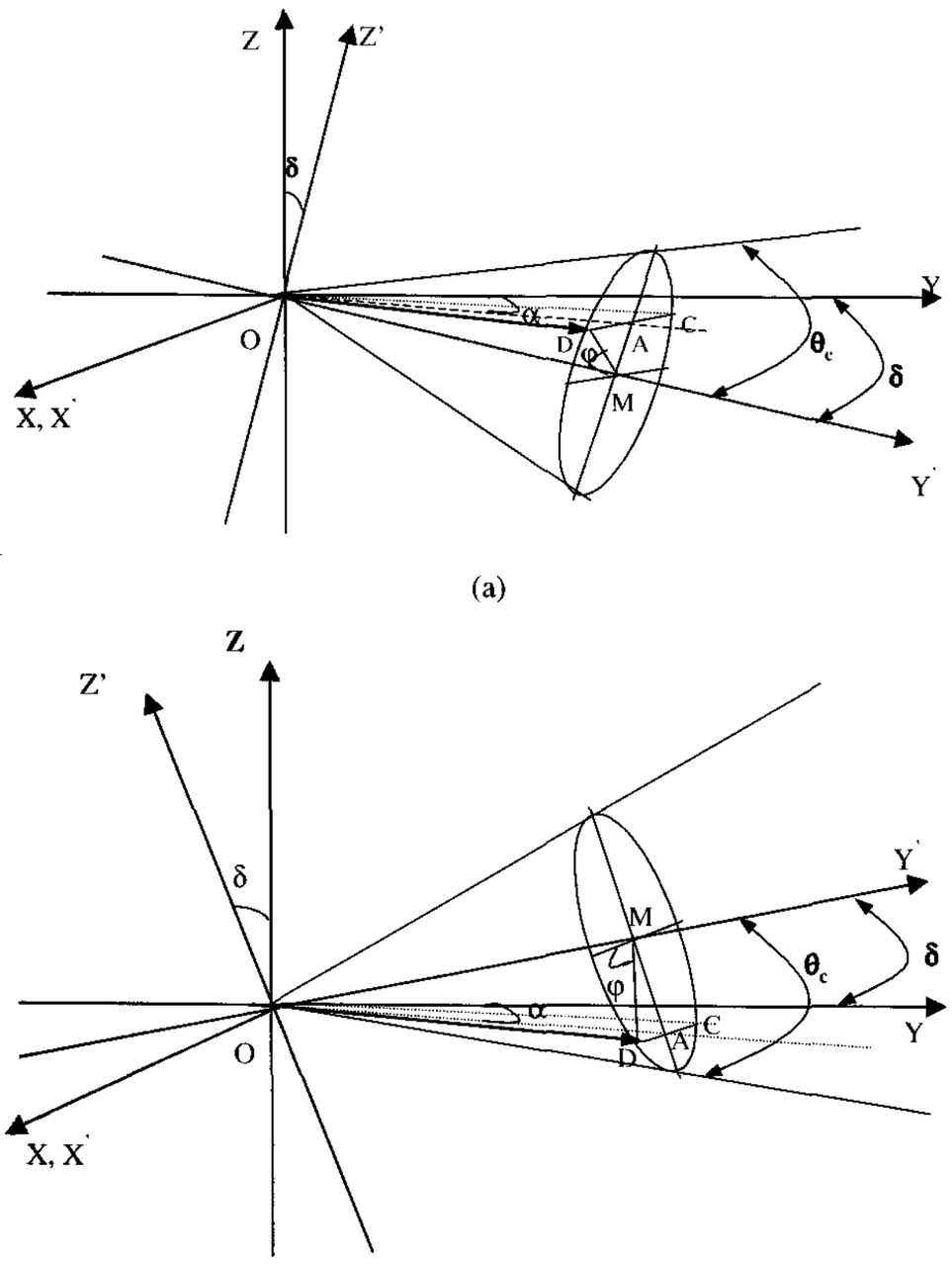

Fig. 3. 3D schematic represenations of the C1 (a) and C2 (b) cone structure in the upper plate of the cell (θ_c: cone angle; δ: layer tilt angle; α: pretilt angle).

$$f_s = W_a \sin^2 \omega \qquad (3)$$

Using the widely applied one elastic constant approximation [13,14] (because the difference between the values of these elastic constants are within a factor of 2-3): $\overline{B} \equiv B_1 = B_2 = B_3$; $B_{13} = D = D_1 = 0$, equation 1 becomes:

$$F = 2 * \left\{ \left[\frac{1}{2} \overline{B} \left(\frac{\varphi_s - \varphi_c}{d/2} \right)^2 \frac{d}{2} \right] + \frac{w_a}{2} \sin^2 \omega \right\} \qquad (4)$$

Where φ_s and φ_c are azimuthal angle φ of the FLC molecules on the bounding plate and chevron interface, respectively.

3.2 Free energy expression of C1 and C2 states

The basic symmetric chevron layer structures of C1 and C2 states are shown in Fig. 1 and Fig. 3. The two boundary plates are equally treated and the rubbing directions of two plates are parallel. We take the **Z**-axis along the cell normal, **Y**-axis along the direction of the projection of the layer normal in the boundary plate, and **X**-axis perpendicular to both **Y** and **Z**. The lower bounding plate and upper bounding plate are located at **Z**=0 and **Z**=d, respectively. The chevron interface is thus located at **Z**=d/2.

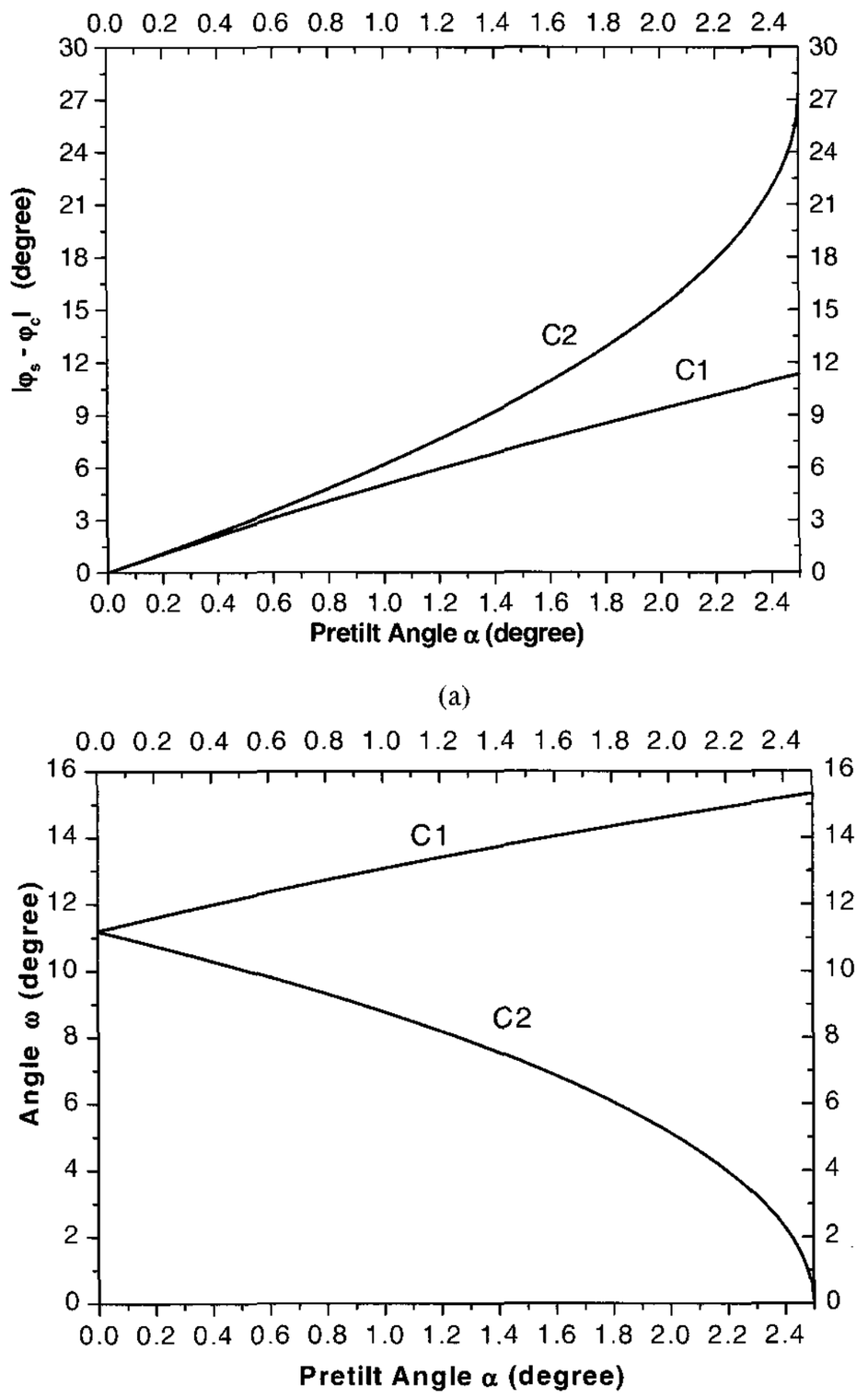

Fig. 4. Plots of $|\varphi_s - \varphi_c|$ vs. pretilt angle (b) and angle ω vs. pretilt angle α (a) for $\delta = 0.9\theta_c$

From the geometry shown in Fig. 3 and through a series of geometrical transformations [15], the final expressions of free energy per unit area with weak azimuthal anchoring boundarycondition for C1 and C2 states (index j=1 or 2) are:

$$F_{cj} = 2 * \left\{ \left[\frac{1}{2} B \left(\frac{\varphi_{sj} - \varphi_{cj}}{(d/2)} \right)^2 \frac{d}{2} \right] + \frac{w_a}{2} \sin^2 \left(\tan^{-1} \left(\frac{\sin\theta_c \cos\varphi_{sj}}{\cos\theta_c \cos\delta + \sin\theta_c \sin\varphi_{sj} \sin\delta} \right) \right) \right\} \qquad (5)$$

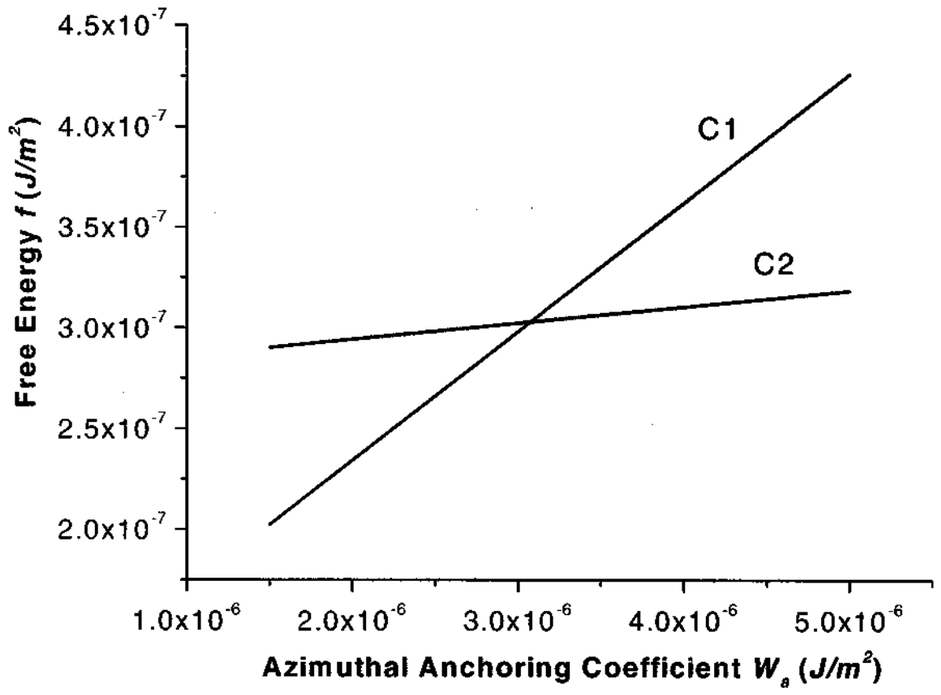

Fig. 5. Free energy density of C1 and C2 vs. azimuthal anchoring coefficient ($\delta=0.9\theta_c$).

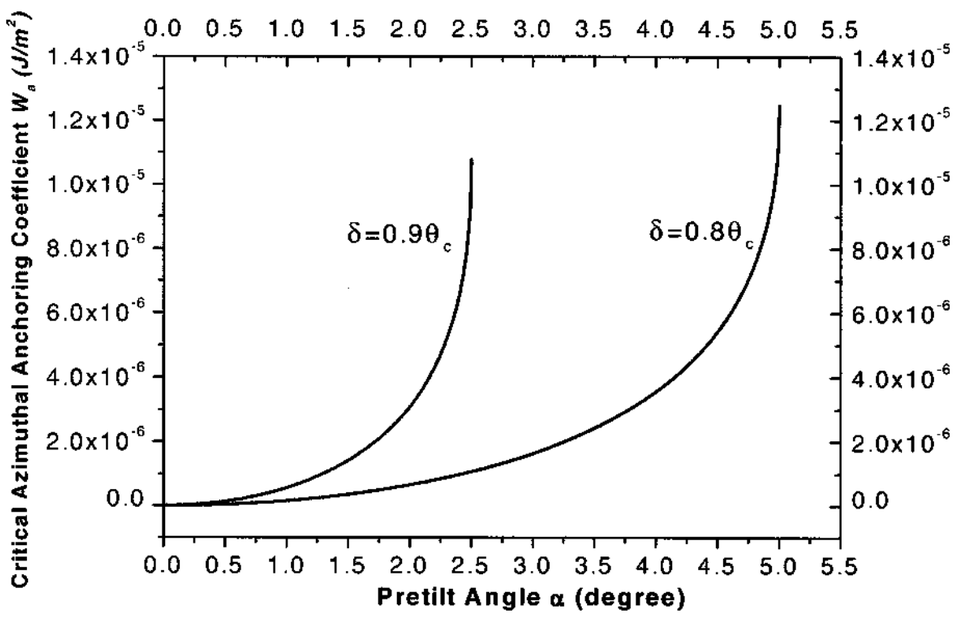

Fig. 6. Critical azimuthal anchoring coefficient vs. pretilt angle α at different chevron angle.

Where $\sin\varphi_{cj}=\frac{\tan\delta}{\tan\theta_c}$, $\sin\varphi_{s1}=\frac{\tan(\delta-\alpha)}{\tan\theta_c}$,

$\sin\varphi_{s2}=\frac{\tan(\delta+\alpha)}{\tan\theta_c}$ θ_c δ, α are cone angle, layer tilt angle and pretilt angle, respectively.

3.3 Discussion

Suppose $\theta_c=25^\circ$ and $\delta=0.9\ \theta_c$, from equation 4 and 5, we plot the relationship between angle ω and pretilt angle α as well as the relationship between "twist sense" $|\varphi_s-\varphi_c|$ and pretilt angle α for C1 and C2 (see Fig. 4). From fig. 4, it is easy to see that the elastic energy of C1 is always less than C2. But azimuthal anchoring energy of C1 is always larger than C2. Both $|\varphi_s-\varphi_c|$ and ω depend on pretilt angle α. Therefore, to get a defect free C1 texture, we should lower the azimuthal anchoring energy part. When azimuthal anchoring coefficient is low enough, C1 becomes the energy-preferred state.

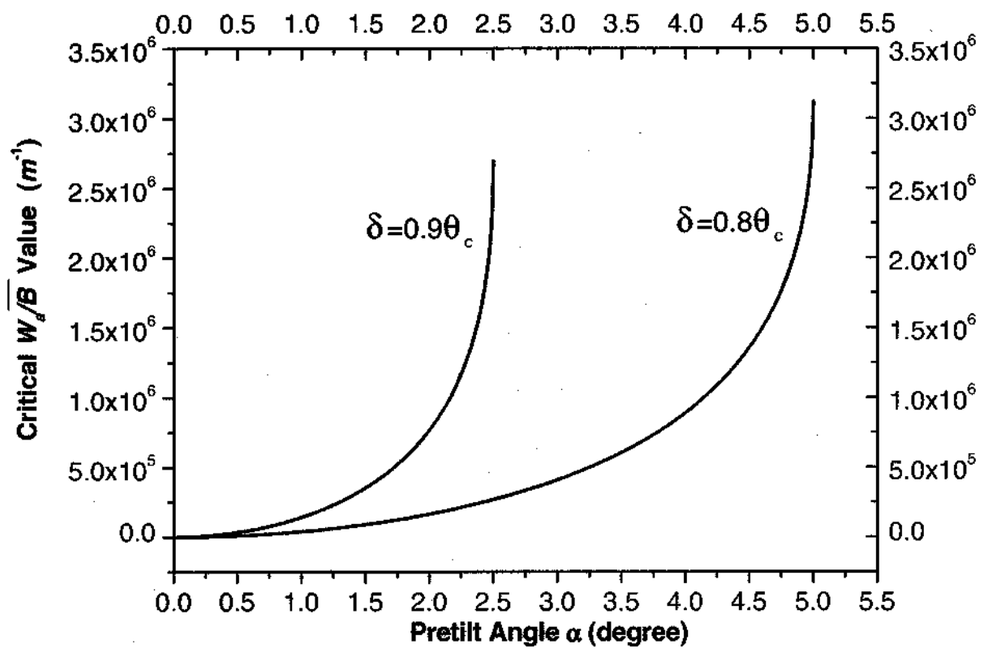

Fig. 7. Critical $W_a/\bar{B}$ vs. pretilt angle α at different chevron angle.

Suppose $\alpha=2^\circ$, d=2 μm, $\bar{B}=4\times10^{-12}$ N, $\theta_c=25^\circ$, we F_{c1} and F_{c2} vs. azimuthal anchoring coefficient W_a (Fig. 5). And it is easy to determine the critical azimuthal anchoring coefficient W_a by setting $F_{c1}=F_{c2}$. (In this case $W_{a\_critical}=3.07\times10^{-6}$ J/m^2 for $\delta=0.9\ \theta_c$). From the relationship between critical W_a and pretilt angle at different chevron angle (Fig. 8), we can see that the critical W_a always increases with the increase of pretilt angle especially when $\delta+\alpha\cong\theta_c$. And at the same pretilt angle, the larger the chevron angle, the larger the critical W_a. On the other hand, Fig. 6 also shows that if the pretilt angle is less than 0.2 °, the critical azimuthal anchoring will be less than 10^{-8} J/m^2, which is really hard to get. It is frequently observed that a C2 structure is obtained with common "high" azimuthal anchoring alignment. Because it has been shown [6, 7, 16] that SmC does exist from C1 state near the SmA-SmC* transition, the anchoring energy of common alignment material causes a transition from the C1 to C2 states during cooling and occasionally leaves zigzag defects. Since critical W_a is also sensitive to $\bar{B}$, the plot of critical $W_a/\bar{B}$ vs. α is also obtained (see Fig. 9).

From above discussion, we propose that defect free C1 can be achieved at relatively low pretilt ($0.2^\circ<\alpha<\theta_c-\delta$) by using low azimuthal alignment material, which has W_a less than the critical value at that pretilt angle. And the FLC will stay at C1 state during the cooling process since C1 state is the energy-preferred state.

The critical azimuthal anchoring coefficient W_a strongly depends on the pretilt angle α, chevron angle δ as well as elastic constant $\bar{B}$. The larger the α, δ and $\bar{B}$,

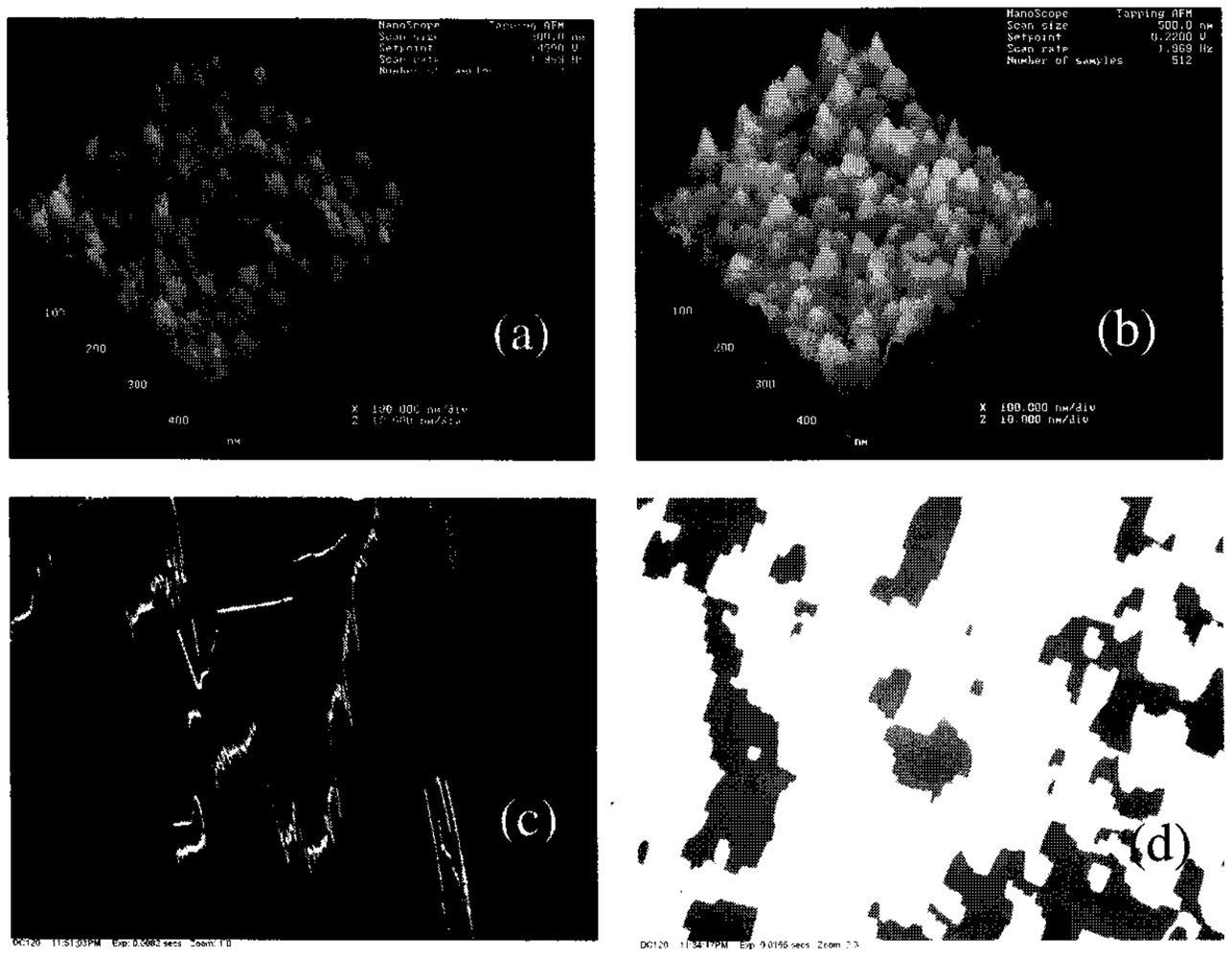

Fig. 8. AFM images of the surface topography of 5 ° oblique SiO deposition and their corresponding microscopic texture. (a) & (c): The AFM picture of SiO with a thickness of about 160 Å and its corresponding zigzag texture (filled with F100). (b) & (d): The AFM picture of SiO with a thickness of about 203 Å and its corresponding zigzag-free texture (F100).

the larger the critical azimuthal anchoring coefficient and subsequently, it is easier to get defect free C1. Since critical W_a is related to α, the surface topography should also be considered at low pretilt angle, which is in agreement with the study done by Watson et al. [8] and the preliminary research done by Kurihara et al. [10] where azimuthal anchoring coefficient is in the range of 10^{-6} J/m^2. Our results further predict that it is possible to get zigzag free C1 device by using low azimuthal anchoring alignment material such as photo alignment of azo dyes or polyimides which normally have uniform smooth surface alignment with $10^{-8}<W_a<10^{-6}$ J/m^2. Our result is consistent with the experiments reported recently [17].

4. Defect Free C1 with a High Pretilt

Using 5 ° obliquely evaporated SiO alignment to get zigzag free C1 has been studied since 1988 [7, 9]. However, this device still generally shows some defects. Our studies focused on how SiO deposition condition and material affect the defect formation.

The cells we used are sandwich type parallel alignment cell with the cell gap ~1 μm. The substrate was ITO glass coated with 5 ° obliquely evaporated SiO as alignment layer. The SiO deposition took place in a high vacuum (10^{-6}-10^{-7} torr) bell jar at room temperature. The SiO boat was a multi-heat-baffled, tantalum boat. The incident angle is 5 degree (85 degree to the cell normal). The amount of silicon oxide evaporated during the deposition was monitored by an Inficon XTM/2 deposition monitor using a sensor-crystal (Gold, 6 MHz), which is situated directly above the boat. The substrates were located about 73 cm from the source. The deposition rate is about 2-5 Å/sec. The final SiO thickness is calibrated by an ellipsometer. The cell is assembled with parallel alignment. The FLC was filled in isotropic state in vacuum and cooled down very slowly (<2 °C/min) to room temperature. The FLCs we used in the experiments are Felix-019-000 (F000) and Felix-019-100 (F100) from Clariant. Their physical properties are shown in Table 1.

4.1 Defects related to the SiO alignment

4.1.1 SiO deposition condition vs. zigzags

The major defect for SiO aligned SSFLC display is zigzag. In our case, we found that zigzag defects are

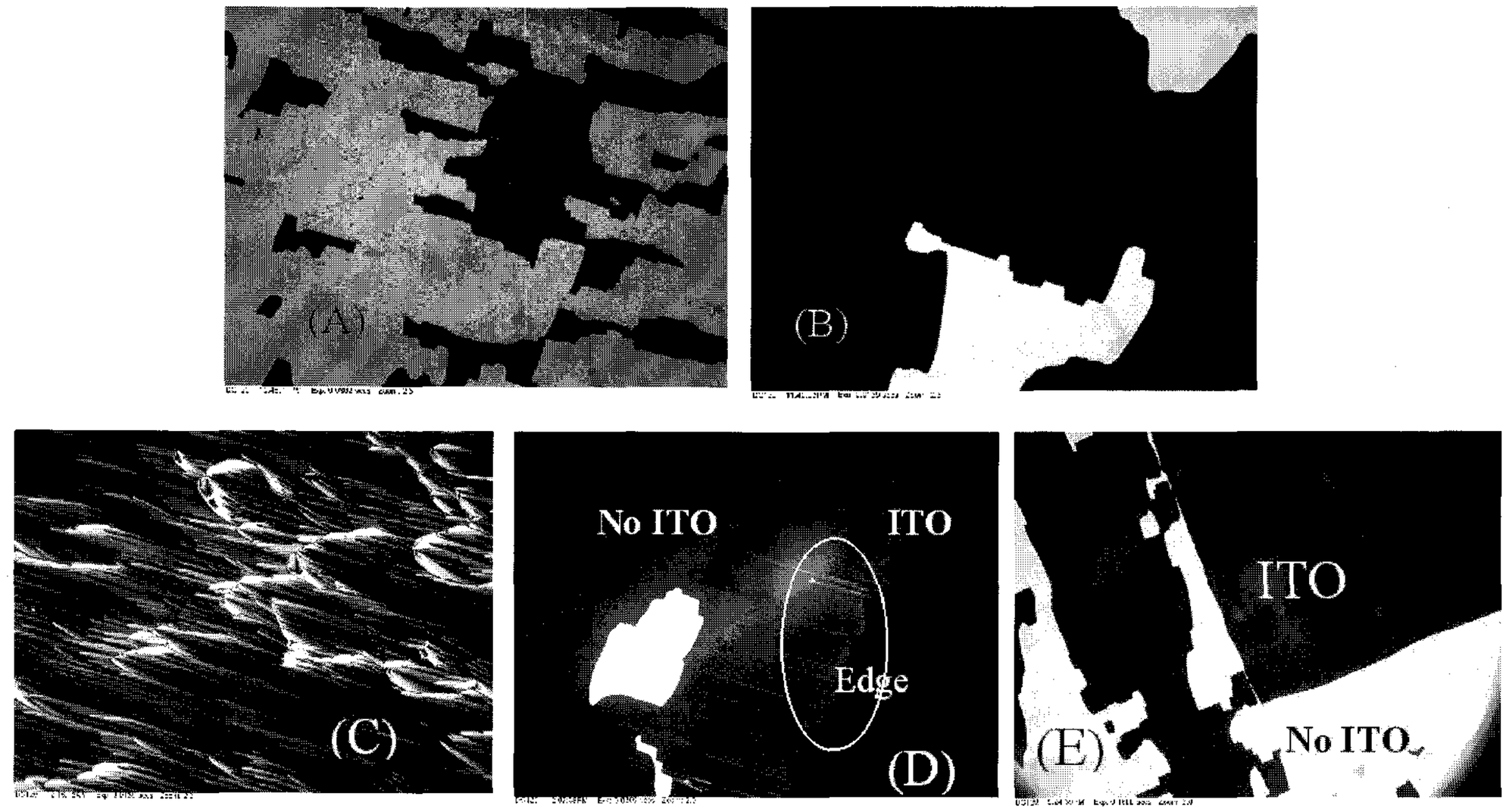

Fig. 9. The microscopic textures of the cells with and without spacers. For F000: (A) The cell with spacers, (B) Spacer in glue edge only; For F100: (C) The Pin defects around the spacers, (D) Pin defects around unevenly etched ITO edge. (E) The total defect-free texture around the pixel edge after optimizing the etching condition and putting spacers in glue edge only.

Table 1. Physical Properties of Felix-019-000 and-100

Properties	Felix-019-000 (F000)	Felix-019-100 (F100)
Phase sequence	X 2 SmC^* 60 S_A76 N^* 82-81 I	X -10 SmC^* 64 S_A 78 N^* 87-84 I
*P*s (nC/cm^2)	8.3	39

directly related to the thickness of SiO and deposition condition. Since SiO deposition is a sublimation process instead of melting and evaporation, to get amorphous film with small grain size and good adhesion to substrate, a multi-heat-baffled, tantalum heating boat should be used to prevent spitting and scattering, which can cause pinholes on the substrate. Because of the tendency of SiO to disproportionate when heated to excessive temperature, alignment layer deposited at high rates, low pressure and low oxygen partial pressure will contain free crystalline silicon ($2SiO \leftrightarrow 2Si+O_2$), which will be dark in color due to the strong UV and blue light absorption by the free silicon. Normally, a good alignment film has an oxidation state between SiO and SiO2. Film obtained by fast evaporation and/or at pressure below 10^{-5} torr is close to SiO (n=1.96), while films obtained by slow evaporation and/or high oxygen pressures is close to SiO_2 (n_{sio2}=1.463). Therefore control of the deposition parameters during oblique deposition turns out to be very important [18].

In addition, the thickness of SiO is also important. Fig. 8 shows how the surface topography for 5 ° SiO deposition is related to the alignment texture of F100. Fig. 8 (a) is the AFM image of SiO with thickness about 160 Å. Fig. 8 (c) is the corresponding texture seen in the microscope. The zigzag defects come out randomly due to the non-uniformity of SiO columns. Fig. 8 (b) and (d) correspond to the AFM image of SiO with thickness ~203 Å and its alignment texture, respectively. The uniform column creates the high pretilt angle, which is about 34 ° measured from magnetic null method using ECB cell filled with 5CB. When the SiO has a thickness

>250 Å, the chance to get the zigzag defects increases and the liquid crystal is easy to form bubbles during the vacuum filling because of large surface area of SiO, which can trap a lot of gas. The best SiO thickness we found is around 200-250 Å. The stability of the high vacuum is also important, which controls the uniformity of the SiO alignment.

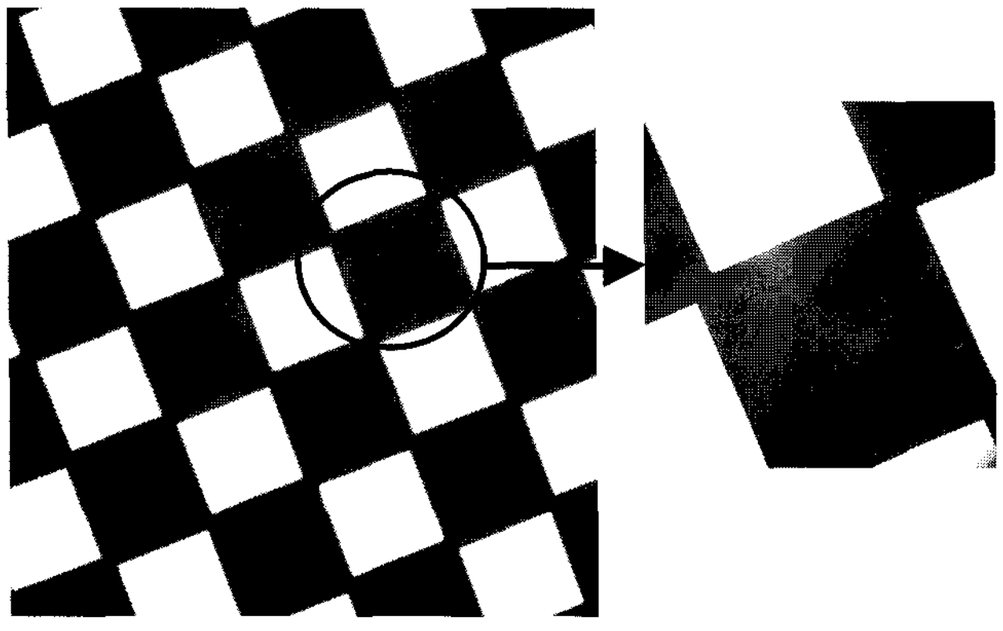

Fig. 10. Left side: Normal transmissive view of the LCD panel through polarizing microscope. Right Side: Magnification of the pixel.

4.1.2 Pin defect related to the spacer and dust

Another defect is the pin defect, which is related to the spacers and the dust and looks like a meteor. We found that the top of the pin defect is a dust particle or a spacer and the tail of this pin defects is always along the alignment direction. The reason for this pin defect is that the spherical silicon spacer "aligns" the SmC* layer and makes it parallel to the sphere surface [18, 19]. The boundary condition of the spacer distorts the smectic layer and produces the defects.

In our case, we found that the F000 is not very sensitive to the presence of spacers, which makes this material very good for direct view SSFLC displays for E-paper device. On the other hand, the spacers cause a lot of pin and focal conic defects for F100. Even the rough ITO etching edge can cause the pin defect. We eliminated this defect by mixing the spacers in the UV-curable glue instead of spraying spacers onto the whole substrate and properly controlling the etching condition. The pin defects are removed and the contrast ratio improved significantly. The textures of the cell before and after removing the spacers from the pixel region for both materials are shown in Fig. 9. We found that the pin defect actually starts from the SmA phase. But how pin defect is related to the material properties is still unknown and is under our investigation. We will report it later.

4.2 Conclusion

For high pretilt SiO alignment, We removed the zigzag defects by optimizing the SiO thickness, uniformity, deposition condition and pretilt angle. The less sensitivity of spacers for F000 makes it suitable for direct view matrix display, such as e-paper. We made a 2 by 2 inch 200 x 200 lines matrix display shown in Fig. 10. . The demo shows very good bistability and high contrast ratio (> 250:1). The memory angle 2 θ_{mem} is about 38 degree at zero field and the switching angle is about 40 degree with field. If voltage supply is higher than 23 volts, the minimum pulse width is below 100μs. We can expect that the line time is less than 300 μsec by using 3-phase waveform, and full page addressing can be achieved under 0.3 sec. This makes it a very promising candidate for electronic paper application.

The spacers-in-glue-edge method limits the size of the display. But it is suitable for microdisplays. The pin defects can also be removed by patterned spacers at the inter-pixel region, which can be used for large size direct view display. These improvements lead to our defect-free bistable SSFLC display.

References

[1] D.K. Yang and J.W. Doane, Proc. Soc. Inf. Disp. 1, 759 (1992).

[2] Ph. Mariinot-Lagarde and et. al., Proc. Soc. Inf. Disp. **1**, 41 (1997).

[3] H. Kuma, T. Iwakuma, F. Moriwaki, and M. Fukuda et. al., Proc. Soc. Inf. Disp., San Jose, 12 (2001).

[4] N.A. Clark and S.T. Lagerwall, Appl. Phys. Lett. **36**, 899 (1980).

[5] H. Furue, Y. Iimura, Y. Miyamoto, H. Endoh, H. Fukuro, and S. Kobayashi, Mol. Cryst. Liq. Cryst. **328**, 193 (1999).

[6] M. Koden, H. Katsuse, A. Tagawa, K. Tamai, N. Itoh, S. Miyoshi, and T. Wada, Jpn. J. Appl. Phys., Part 1 **31**, 3632 (1992).

[7] J. Kanbe, H. Inoue, A. Mizutome, Y. Hanyuu, K. Katagiri, and S. Yoshihara, Ferroelectrics **114**, 3 (1991).

[8] P. Watson, P. J. Bos, and J. Pirs, Phys. Rev. E **56**, R3769 (1997).

[9] P. J. Bos and K. R. Koehler/Beran, Ferroelectrics **85**, 15 (1988).

[10] R. Kurihara, H. Furue, T. Takahashi, and S. Kobayashi,

Proc. Soc. Inf. Disp., **31**, 807 (2000).
[11] J. L. Janning, Appl. Phys. Lett. **21**, 173 (1972).
[12] T. Akahane, K. Itoh, and N. Nihei, Jpn. J. Appl. Phys., Part 1 **32**, 5041 (1993).
[13] S. T. Lagerwall, Ferroelectric and Antiferroelectric Liquid Crystals (Wiley-VCH, Weinheim, 1999), Ch. 11.
[14] W. H. de Jeu, Physical Properties of Liquid Crystalline Materials (Gordon and Breach, New York, 1980), Ch. 6.
[15] C. Wang, R. Kurihara, P. J. Bos, S. Kobayashi, J. Appl. Phys. **90**: (9) 4452 (2002)
[16] J. Xue, in Proceedings of SPIE-the International Society for Optical Engineering (1996), p. 10.
[17] R. Kurihara, H. Furue, T. Takahashi, et al., Jpn. J. Appl. Phys. 1 **40**: (7) 4622 (JUL 2001).
[18] C. Wang, P. J. Bos, M. Wand, and M. Handschy, Soc. Inf. Disp. (SID) 2002 Digest, **33**, 34 (2002).
[19] J. Xue, Ph. D thesis, University of Colorado, Boulder, USA (1989)